31st Annual International Conference of the IEEE EMBS
Minneapolis, Minnesota, USA, September 2-6, 2009

Quantitative Spectral Reflectance Imaging Device for Intraoperative Breast Tumor Margin Assessment

Nimmi Ramanujam, J. Quincy Brown, Torre M. Bydlon, Stephanie A. Kennedy, Lisa M. Richards, Marlee K. Junker, Jennifer Gallagher, William T. Barry, Lee G. Wilke, Joseph Geradts

Abstract—**Diffuse reflectance spectroscopy of tissue allows quantification of underlying physiological and morphological changes associated with cancer, provided that the absorption and scattering properties of the tissue can be effectively decoupled. A particular application of interest for tissue reflectance spectroscopy in the UV-VIS is intraoperative detection of residual cancer at the margins of excised breast tumors, which could prevent costly and unnecessary repeat surgeries. Our multi-disciplinary group has developed an optical imaging device, which employs a model-based algorithm for quantification of tissue optical properties, and is capable of surveying the entire specimen surface down to a depth of 1-2 mm, all within a short time as required for intraoperative use. In an ongoing IRB-approved study, reflectance spectral images were acquired from 55 margins in 48 patients. Conversion of the spectral images to quantitative tissue parameter maps was facilitated by a fast scalable inverse Monte-Carlo model. Data from margin parameter images were reduced to image-descriptive scalar values and compared to gold-standard margin pathology. Use of a decision-tree based classification algorithm on the two most significant optical parameters resulted in a sensitivity of 79% and specificity of 67% for detection of residual tumor of all pathologic variants, with an 89% sensitivity for ductal carcinoma *in situ* alone. Preliminary data from this ongoing clinical study suggest that this technology could significantly reduce the number of unnecessary repeat breast conserving surgeries annually.**

I. Introduction

Over the past 30 years, increased patient awareness and advances in breast cancer screening have proven effective in diagnosing cancer at earlier stages, leading to a need for less aggressive surgical and post-surgical therapies. Multiple randomized clinical trials have previously shown that patients who undergo breast conservation surgery (BCS), for either invasive or non-invasive breast cancers, have equivalent long-term survival to those who undergo mastectomy [1]-[2]. However, although BCS followed by adjuvant therapy can result in equivalent long-term survival to mastectomy, maximum survival benefit is achieved when the cancer is completely removed in BCS and the cancer does not recur [3].

Currently, breast surgeons do not have adequate intraoperative assessment tools to ensure that the cancer has been fully removed at the time of surgery. Generally, the tumor margin (the 2mm rim of tissue at the boundary of the excised mass) must be free of residual tumor to prevent locoregional occurrence. Histopathology is the gold standard for assessing breast tumor margins. However, intraoperative pathology is only available at a handful of breast surgery centers in the US. This lack of intraoperative margin assessment has resulted in a reported 20-70% [4] of the 180,000 patients undergoing BCS annually to be subjected to additional surgeries to remove residual tumor left behind at the first surgery.

In order to provide a tool for assessing breast tumor margins intra-operatively and thereby reduce the re-excision and local recurrence rate, we have developed a device which utilizes optical spectral imaging to characterize differences in tissue composition of excised breast specimen margins. This device utilizes the primary light-tissue interactions of absorption and scattering in the visible part of the electromagnetic spectrum to characterize the underlying tissue composition. The sources of intrinsic optical contrast can be broadly classified as morphological (β-carotene, cell and organelle density) and physiological (deoxygenated and oxygenated hemoglobin and total hemoglobin content). A number of these biomarkers are hallmarks of carcinogenesis and provide an effective means for detecting residual tumor at the margin. Herein we report on the development of the optical tumor margin imaging device and preliminary results from 48 patients in an ongoing 150+ patient study.

II. Materials and Methods

A. Instrumentation

The optical imaging device consists of a Xenon lamp coupled to a double monochromator (Gemini 180, Jobin-Yvon HORIBA), a custom-built 8-channel fiber-optic imaging probe (RoMack, Inc) interfaced to an adjustable tissue specimen container, and an imaging spectrograph (Triax 320) and a 16-bit TE-cooled CCD camera (Symphony) (both from Jobin-Yvon HORIBA). This system can be used to measure diffuse reflectance spectra as well as multi-excitation fluorescence spectra from 8 discrete sites simultaneously. However, in this report the illumination

Manuscript received June 4, 2009. This publication was made possible by Grant Number 1UL1 RR024128-01 from the National Center for Research Resources (NCRR), a component of the National Institutes of Health (NIH), and NIH Roadmap for Medical Research. Its contents are solely the responsibility of the authors and do not necessarily represent the official view of NCRR or NIH.

Nimmi Ramanujam is with the Biomedical Engineering Dept. at Duke University. (919-660-5307; fax: 919-684-4488; e-mail: nimmi@duke.edu).

monochromator was set to zero-order diffraction to achieve white-light illumination for diffuse reflectance measurements only. The common end of each channel of the probe consists of a central illumination core (~1 mm diameter) composed of 19 close-packed illumination fibers surrounded by 4 collection fibers. All fibers have a diameter of 200 μm with a numerical aperture (NA) of 0.22. The typical power output at the probe tips is ~3 μW and 25 μW with a 10 nm bandpass at 450 and 600 nm (the limiting wavelengths of the spectrum), respectively. At the illumination end of the probe, all 152 illumination fibers are packed in a linear array for efficient coupling with the exit slit of the monochromator. At the collection end, the 4 collection fibers from each channel are bundled into 2×2 arrays, which were further packaged into a vertical linear array with 2 dead fiber spacing between each adjacent 2×2 array. The latter arrangement was designed to avoid crosstalk between adjacent collection channels on the CCD. Light collected at the entrance slit of the spectrograph (set at 2.2 mm) was diffracted by a 600 line/mm grating and projected onto the 1024×256 CCD, resulting in a spectral resolution of 2.5 nm. With this particular grating, two sequential scans were required to cover the full wavelength range of interest (450-600 nm). The CCD integration time for each scan was optimized independently to obtain the highest reflectance signal possible while staying within the linear operation limits of the CCD.

B. Margin Imaging

The imaging probe was interfaced to the lumpectomy specimen through an acrylic container, with holes drilled for insertion of each channel of the probe, allowing the probe tips to just come in contact with the tissue. A center-to-center spacing of 5 mm was used for the specimen box, but the 8-channels of the imaging probe were secured in an aluminum chuck in a 4×2 array with 10mm center-to-center spacing to prevent crosstalk between adjacent probes. The excised breast tumor specimens were oriented by the surgeons, who used a system of sutures and surgical clips to identify the superior and lateral margins (from which all other margins can be identified). The specimens were placed into the container such that the orientation was maintained. On average, margins were imaged 18 ± 5 minutes after excision. The imaging probe was interfaced with the tissue by inserting the probe tips into the holes of the container. Figure 1 contains a photograph of the imaging probe interfaced with the specimen container during imaging of a lumpectomy specimen. The probe tips are designed such that they extend about 1 mm past the inner surface of the container, providing a reproducible probe-tissue contact. A single placement of the probe array collects data from 8 container holes (or pixels). The entire margin surface was imaged by manually translating the position of the imaging probe horizontally and vertically until data from all of the pixels were obtained.

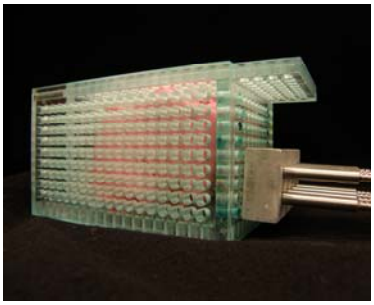

Figure 1. A close-up photograph of a specimen mock-up being imaged by the handheld probe.

C. Spectral Processing and Image Analysis

A custom software application was written in-house using LabVIEW 8.5 (National Instruments, Austin, TX) and MATLAB R2008a (Mathworks, Natick, MA). This application was used to control the flow of information from instrument initialization to image display, providing automated selection of data acquisition parameters, data post-processing, and output of results to the operator, as well as providing data quality-control functions. Measured reflectance spectra from each pixel were pre-processed by dividing point-by-point by a spectrum from a 99% reflectance standard (LabSphere), and then were fed into the fast scalable inverse Monte Carlo model for extraction of wavelength-dependent tissue scattering and absorption coefficients, and computation of constituent absorber concentrations and wavelength-averaged scattering coefficients as previously described [5]-[6]. The dimensions of margins imaged thus far in the 48 patients ranged from 2 cm × 2 cm to 4.5 cm × 9.5 cm. For a small margin, approximately 4 placements of the probe were required to image the entire margin (requiring up to 100s total acquisition and processing time), and for a large margin up to 16 placements were required (requiring up to 400s total acquisition and processing time).

Images of the margins were reconstructed with the extracted absorber concentrations and scattering parameters. In addition to maps of the concentrations of oxy- and deoxy-hemoglobin and β-carotene, and the wavelength-averaged reduced scattering coefficient, $\langle \mu_s' \rangle$, maps of the ratios of absorber concentrations and $\langle \mu_s' \rangle$ were also computed. To reduce the images to scalar values for automated classification, histograms of the image data were computed, and thresholds were empirically determined and applied to the histograms that efficiently separated images of positive margins from images of negative margins. Wilcoxon rank-sum tests were used to determine which variables were most effective at separating negative from positive margin images.

D. Pathologic Co-registration and Margin Classification

Following imaging of the full margin surface, the four corners of the imaged margin were inked with a standard insoluble ink to establish its boundaries such that the pathologist could evaluate areas within the same region of interest for margin-level pathology. The margin-level diagnoses of the surgical margins of the primary surgical specimen were obtained from the post-operative pathology

report. For the purposes of this study, margins that were classified by pathology as positive (cancer extending to the surface) or close (cancer within 2 mm of the surface) were classified as positive, since the clinical implication for both positive and close margins is equivalent.

III. Results

Figure 2 contains sample optical parameter maps for a margin positive for residual disease as well as a cancer-free margin. These particular maps are of the ratio of β-carotene concentration to $<\mu_s'>$, in which lower values (rendered red) indicate areas of less fat and higher scattering (indicative of the presence of cancer), whereas higher values (rendered blue) indicate areas of more fat and lower scattering (indicative of normal breast tissue). Clear differences are observed between the 2 margins. The central red area in Figure 2A was confirmed to be an area of residual disease, whereas no residual disease was found in the margin of Figure 2B. β-carotene is a carotenoid primarily stored in fatty tissues, and may thus be considered as a surrogate for fat content.

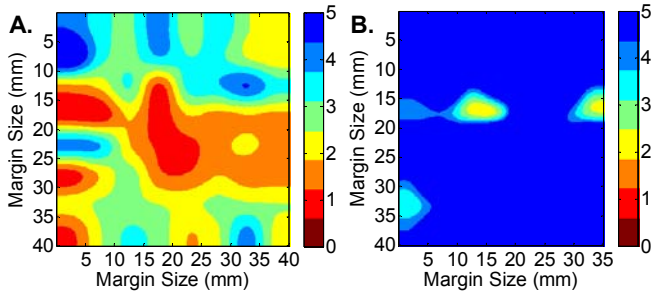

Figure 2. Maps of [β-carotene] / $<\mu_s'>$ for A) a path-confirmed margin positive for invasive ductal carcinoma and ductal carcinoma *in situ*, and B) a path-confirmed negative margin (free of residual disease).

Wilcoxon rank-sum analysis of all margin parameter maps indicated two variables which exhibited the most significant differences between negative and positive margins. These variables were the ratios β-carotene / $<\mu_s'>$ and [total hemoglobin] / $<\mu_s'>$. The concentration of total hemoglobin is indicative of vascular volume and hence may be reflective of angiogenesis. Both parameters exhibited statistically significant differences ($P < 0.01$) between positive and negative margins.

Next a multivariate predictive model was developed for classifying a margin as positive or negative based on the predictors. A tree-based approach was taken to build the two-parameter model, such that a margin was classified as positive if the percentage for the β-carotene / $<\mu_s'>$ *or* total hemoglobin / $<\mu_s'>$ parameters were above their respective thresholds; otherwise it was classified as negative. The percentages were each varied across the complete set of different threshold values, and the sensitivity and specificity was then calculated against margin assessment by pathology. The optimal pair of threshold values was determined by a receiver operator characteristic analysis, and the Youden index, in order to maximize the sensitivity and specificity in an additive manner. Then, a leave-one-out cross validation scheme was used to obtain an unbiased estimate of the operating characteristics of the predictive model using the same guiding principles as above, and resulted in a sensitivity and specificity of 79% and 67%, for the two parameter decision tree.

IV. Discussion and Conclusion

In this short paper, we described the development of a reflectance spectral imaging device for breast tumor margin assessment and preliminary results from 48 patients. Using a decision-tree based predictive model and reducing image data to scalar values using a thresholding scheme, the device was able to detect positive margins, regardless of pathology or depth from the margin, with 79% sensitivity, with a corresponding 33% false-positive rate. Interestingly, the device correctly identified 8 of 9 margins positive for ductal carcinoma *in situ* (DCIS) which corresponds to a sensitivity of 89%. Detection of DCIS intraoperatively is particularly important, since DCIS presents a challenge for surgeons due to its low mammographic density (making it difficult or impossible to see in specimen radiographs), as well as its indistinct gross characteristics. These promising preliminary results suggest that the device presented here could provide a useful tool for objective, intraoperative guidance of breast conserving surgery. Future work will include analysis of data from the remaining patients in the 150+ study cohort.

References

[1] Poggi MM, Danforth DN, Sciuto LC, Smith SL, et al. Eighteen-year results in the treatment of early breast carcinoma with mastectomy versus breast conservation therapy: the National Cancer Institute Randomized Trial. Cancer, 2003; 98: 697-702.

[2] Fisher B. Highlights from recent National Surgical Adjuvant Breast and Bowel Project studies in the treatment and prevention of breast cancer. CA Cancer J Clin., 1999;49: 159-77.

[3] Clarke M, Collins R, Darby S, et al. Effects of radiotherapy and of differences in the extent of surgery for early breast cancer on local recurrence and 15 year survival: An overview of the randomized trials. Lancet, 2005; 366: 2087–2106.

[4] Jacobs LJ. Positive Margins: The Challenge Continues for Breast Surgeons. Ann Surg Onc, 2008; 15: 1271-1272.

[5] Palmer GM, Ramanujam N. Monte Carlo-based inverse model for calculating tissue optical properties. Part I: Theory and validation on synthetic phantoms. Appl Opt, 2006; 45: 1062-71.

[6] Palmer GM, Ramanujam N. Monte Carlo-based inverse model for calculating tissue optical properties. Part II: Application to breast cancer diagnosis. Appl Opt, 2006; 45: 1072-1078